Applied Catalysis A, General 724 (2026) 121065

Contents lists available at ScienceDirect

Applied Catalysis A, General

journal homepage: www.elsevier.com/locate/apcata

In situ X-ray absorption spectroscopy to study redox dynamics in Ni and Cu co-catalysts on porous TiO_2 photocatalyst films during H_2 evolution

Marco Pinna [a,b,c,1], MemetTursun Abudukade [b,1], Viktoriia A. Saveleva [d,e], Davide Spanu [a], Xiufang He [f], Sandro Recchia [a], Alessandro Minguzzi [f,g], Guido Mul [b], Paolo Ghigna [h], Marco Altomare [b,*]

[a] Department of Science and High Technology, University of Insubria, Via Valleggio 11, Como 22100, Italy
[b] Department of Chemical Engineering, MESA+ Institute for Nanotechnology, University of Twente, P.O. Box 217, Enschede 7500 AE, the Netherlands
[c] Nano and Molecular Systems Research Unit, University of Oulu, Penti Kaiteran katu 1, Oulu 90570, Finland
[d] European Synchrotron Radiation Facility (ESRF), 71 Avenue des Martyrs, Grenoble 38000, France
[e] Labcom Li, LEPMI, Blue Solutions, 1025 rue de la Piscine, Gières 38610, France
[f] Dipartimento di Chimica, Università degli studi di Milano, Milan 20100, Italy
[g] UdR INSTM di Milano - Consorzio Interuniversitario Nazionale per la Scienza e Tecnologia dei Materiali – INSTM, Via G. Giusti 9, Firenze 50121, Italy
[h] Dipartimento di Chimica, Università degli Studi di Pavia, Via Taramelli 16, Pavia 27100, Italy

ARTICLE INFO

Keywords:
In situ XAS
Photocatalysis
Hydrogen
TiO_2
Co-catalyst
Nickel
Copper
Sputtering

ABSTRACT

Bimetallic NiCu co-catalysts are consistently reported to be more active than monometallic Ni and Cu counterparts for photocatalytic H_2 evolution. There is consensus in the literature that this effect is due to the NiCu electronic structure, which provides an optimal adsorption/desorption energy landscape for faster H_2 evolution kinetics compared to monometallic co-catalysts. Less is known, however, about the oxidation state of Ni and Cu co-catalysts under photocatalytic conditions, both in the case of mono- and bi-metallic systems. Red-ox dynamics for Ni and Cu are particularly complex in liquid aqueous media where, in addition to changes in oxidation state induced by photogenerated charge carriers, Ni and Cu can undergo dissolution, redeposition and surface reconstruction. Several diverging hypotheses on Ni and Cu oxidation states have been formed in recent years, most of which were based primarily on results of *ex situ* characterization techniques. Herein, we use *in situ* X-ray Absorption Spectroscopy to investigate red-ox dynamics in Ni-, Cu-, and NiCu-TiO_2 photocatalysts in plain water and water/methanol solutions under hydrogen evolution conditions. This enables us to monitor changes in Ni and Cu oxidation state over time and identify the active phase of Ni and Cu co-catalysts "at work". It is proposed that the observed synergy in NiCu-TiO_2 arises from a division of roles, where Cu serves as an efficient electron sink for hydrogen evolution, while Ni acts as a dynamic hole buffer through reversible oxidation, thereby enhancing charge separation and suppressing self-deactivation pathways.

1. Introduction

Metal co-catalysts are an essential component of semiconductor based photocatalysts when used in photocatalytic evolution of hydrogen and oxygen by decomposition of H_2O. Metal co-catalysts improve interfacial charge transfer and lower the activation energy for the formation of hydrogen, and/or oxygen. Particularly, the formation of oxygen requires high over-potentials. Therefore, often oxidation of hydrocarbons, such as methanol, is used to fundamentally study limitations in photocatalytic hydrogen evolution rates. In this context, high-surface area porous TiO_2 materials, surface-modified with noble metal co-catalysts (e.g., Pt, Pd, Au) evolve H_2 from alcohol-water mixtures at higher rates than from plain water under UV light illumination, demonstrating that oxygen evolution is limiting the rate of photocatalyzed decomposition of H_2O to H_2 and O_2. [1,2] The low abundance of noble metal co-catalysts has shifted research towards more abundant

* Corresponding author.
E-mail addresses: marco.pinna@oulu.fi (M. Pinna), m.r.abudukade@utwente.nl (M. Abudukade), viktoriia.saveleva@blue-solutions.fr (V.A. Saveleva), davide.spanu@uninsubria.it (D. Spanu), xiufang.he@unimi.it (X. He), sandro.recchia@uninsubria.it (S. Recchia), alessandro.minguzzi@unimi.it (A. Minguzzi), g.mul@utwente.nl (G. Mul), paolo.ghigna@unipv.it (P. Ghigna), m.altomare@utwente.nl (M. Altomare).
[1] Authors have equal contributions

https://doi.org/10.1016/j.apcata.2026.121065
Received 31 March 2026; Received in revised form 27 May 2026; Accepted 29 May 2026
Available online 1 June 2026

metals such as Ni and Cu to enhance the photocatalytic hydrogen evolution rate of TiO_2. [3–7] Unfortunately, Ni and Cu typically show instability in photocatalytic reactions. The origin of such instability is not entirely clear. [3,8–10] Early studies on NiO/Ni-$SrTiO_3$ systems suggest that Ni@NiO core shell particles are essential for hydrogen evolution. [9,11] Crozier and coworkers demonstrated by *ex situ* microscopy that the metallic Ni core shrinks during photocatalytic water splitting, deactivating the photocatalytic performance. Besides the role of Ni@NiO core shell particles, other studies propose a different role of Ni, consisting of separated Ni and NiO nanoparticles, where metallic Ni catalyzes HER, while OER is catalyzed by NiO. [10]

In addition to studies on Ni/NiO co-catalysts, Muñoz-Batista and coworkers developed an *in situ* gas phase spectroscopic cell to investigate Cu, and NiCu-TiO_2 photocatalyst powders for H_2 evolution. [12] When the photocatalyst was exposed to methanol-water vapors, they observed metallic Cu under dark conditions while Cu oxidizes to Cu(II) under illumination. On the contrary, Ni was found to be in an oxidized Ni(II) state, and negligible changes in oxidation state occurred when switching from dark to light conditions. More recent *in situ* studies in liquid phase systems reveal light-induced morphological reconstruction and compositional changes of the co-catalysts, and their correlation with the photocatalytic activity. [13,14] Co-catalyst dissolution in water-alcohol mixtures was observed in the dark (forming $Ni^{2+}_{(aq.)}$ or $Cu^{2+}_{(aq.)}$ species), followed by UV light-induced healing of the co-catalyst, i.e., photo-deposition of metallic Ni or Cu particles onto TiO_2, causing a gradual increase of the H_2 evolution rate. In the presence of a hole scavenger (i.e., when holes are rapidly consumed), metallic Ni and Cu were hence suggested to be the active sites for H_2 evolution. Differently, UV illumination of slurries of reduced (sub-stoichiometric) TiO_2 powders in the presence of dissolved Ni(II) salt in plain water (no hole scavengers) was found to form metastable Ni(I) species, likely on the TiO_2 surface, that were active toward H_2 generation, as probed by *in situ* X-ray Absorption Spectroscopy (XAS) and Electron Pair Resonance (EPR) spectroscopy. [15]

The conclusions drawn by these *in situ* studies must be compared carefully, bearing in mind particularly the different reaction conditions. Red-ox dynamics for Ni and Cu are more complex in liquid aqueous media than in gas-phase reactions. In the former case, in addition to changes in oxidation state induced by photogenerated charge carriers, Ni and Cu can undergo dissolution, redeposition, and surface reconstruction. In any case, these findings highlight the importance of *in situ* characterization techniques to identify the oxidation state of metal co-catalysts under operation, thus, to uncover charge carrier dynamics in photocatalytic hydrogen evolution.

In this study, we use *in situ* XAS to investigate red-ox dynamics in Ni, Cu, and NiCu co-catalysts on porous TiO_2 in plain water and water/methanol solutions under hydrogen evolution. We synthesized porous TiO_2 layers and modified them with nanocrystalline Ni, Cu, and bimetallic NiCu co-catalyst thin films via magnetron sputtering. To evaluate their photocatalytic activity, we utilized a continuous stirred-tank reactor (CSTR) coupled with an online gas chromatograph. This setup, as shown in previous work, [13] provides a 2-minute time resolution for online gas analysis. Photocatalytic tests confirm that NiCu-TiO_2 outperforms monometallic counterparts, i.e., Ni-TiO_2 and Cu-TiO_2, in line with previous work, [16,17] while all photocatalysts showed stable H_2 generation over ca. 3 h-long UV irradiation tests and no O_2 evolution. For the spectroscopic investigation, we use a custom-made liquid phase cell for *in situ* XAS in fluorescence mode at the Ni and Cu K-edges. To address spectral distortions due to the co-catalyst films' self-absorption and nanocrystalline nature, we introduce a semi-quantitative method based on spectra peaks' ratio. This enables us to monitor changes in Ni and Cu oxidation state over time and, more importantly, to identify the active phase of Ni and Cu co-catalysts under reaction conditions. Furthermore, we formulate hypothesis on charge carrier dynamics, catalyst surface reconstruction and nature of active sites for Ni-, Cu-, and NiCu-TiO_2 by analyzing the time-resolved XAS spectra in relation to the H_2 evolution rate measured online upon UV light on/off cycles and the changes in co-catalyst morphology. Overall, the *in situ* spectroscopy approach we present enables a step forward in the investigation of photocatalytic systems at work.

2. Experimental

2.1. Preparation of porous TiO_2 photocatalyst layers

The supported porous TiO_2 layers were prepared by electrochemical anodization of Ti foils in fluoride containing organic electrolytes. This experimental approach was chosen as it allows to form homogeneous porous layers. [18–20] Pieces of Ti foils (Advent Research Materials, 0.125 mm thickness, 99.6 %+ purity) of 15 mm × 15 mm were sequentially degreased and cleaned by sonication in acetone, ethanol, and ultrapure water, then dried under a N_2 stream. The cleaned Ti pieces were then anodized in an ethylene glycol (99% purity, Sigma-Aldrich) electrolyte containing 0.15 M NH_4F (≥ 99.99% purity, Sigma-Aldrich) and 3 vol.% H_2O. For the anodization, a two-electrode configuration was employed, with the Ti foil (15 mm × 15 mm) serving as the working electrode and a platinized Ti mesh as the counter electrode. The Ti foil was bottom-mounted in the cell using an O-ring of 1 cm diameter. Anodization was performed at a potential of 60 V using a DC power supply (PPS−11603, Volcraft), and the duration of the anodic oxide growth was varied to control the thickness of the porous TiO_2 layers. Based on previous work, porous oxide layers with a thickness of ~7–8 μm were found optimal for UV light absorption and photocatalytic activity. [16,21] To remove the residual adsorbed electrolyte, the samples were rinsed with and soaked overnight in ethanol after anodization, followed by drying in a N_2 stream. Finally, the amorphous nanotube layers (geometric surface area of 0.78 cm^2) on Ti substrates were annealed at 450 °C for 1 h in air to induce TiO_2 crystallization into a photoactive anatase phase. [22]

2.2. Sputter deposition of Ni, Cu, and NiCu co-catalyst films

Monometallic Ni and Cu, and bimetallic NiCu films were deposited on porous TiO_2 layers using a magnetron sputter coater (ATC Polaris, AJA International Inc.), equipped with Ni and Cu targets (99.99% purity, AJA International Inc.) powered by 2 DC power supplies (DCXS−1500-4, AJA International Inc.). The working pressure during sputtering was maintained at 4.2×10^{-6} bar. The sputtering rates were determined by sputtering Ni and Cu films, and by co-sputtering bimetallic NiCu films of different thicknesses on SiO_2/Si wafers (University Wafer). The thickness of the sputtered films was measured by X-ray Reflectometry (XRR). The details of the calibration are provided in the Supporting Information, including the sputtering conditions for each film (summarized in Table S1). For simplicity, since all photocatalyst layers were aimed to be coated with a co-catalyst layer of 10 nm nominal thickness, we hereafter refer to the samples as Ni-TiO_2, Cu-TiO_2, and NiCu-TiO_2.

2.3. Ex situ characterization of materials

X-ray diffraction (XRD) was performed using a D2 PHASER diffractometer (Bruker) to examine the crystallographic properties (i.e., phase composition) of the TiO_2. The measurements were carried out with the following parameters: Cu Kα source (λ = 1.5406 Å), step size 0.02°, 0.5 s $step^{-1}$, 2θ scan range 10° – 80° in a Bragg-Brentano geometry.

Grazing-incidence XRD measurements were performed to probe the nanocrystalline nature of the sputtered co-catalyst thin films (Ni, Cu, and NiCu). For this, thicker films, 100 nm-thick, of Ni, Cu, and NiCu were sputtered onto SiO_2/Si wafers (University Wafer). The measurements were performed by employing a Malvern Panalytical Empyrean diffractometer and the following experimental conditions: Cu Kα source (λ = 1.5406 Å), 45°−60° 2θ range, step size of 0.02° with integration

time of 0.88 s step^{-1}, incident angle ψ = 0.44 °. We calculated the average grain size by the Scherrer equation (Eq. 1).

$$\tau = \frac{K\lambda}{\beta \cos\theta} \quad (1)$$

Where τ is the mean grain size, K is a numerical constant (0.94), λ is the employed wavelength (0.154056 nm for Cu Kα), β is the full width half maxima (FWHM), and θ is the value of the Bragg angle.

The morphology of the as-prepared and used photocatalysts was investigated by Field Emission Scanning Electron Microscopy (FE-SEM, JEOL, JSM-7610F).

2.4. Photocatalytic Experiments

The photocatalytic H_2 evolution activity of the Ni-, Cu-, and NiCu-TiO_2 photocatalyst layers was evaluated using an optical glass cuvette reactor (402.013-OG, Hellma). The cuvette was filled with 25 mL of de-ionized water (or a 20 vol% methanol-water mixture) in which the photocatalyst was immersed, fixed on a support. The photocatalyst was illuminated with monochromatic UV light (LED Control 5S, Opsytec, λ = 365 nm) and positioned in the cuvette such that the incident irradiance amounted to 100 mW cm^{-2}. We employed a high photon flux and intermittent illumination cycles (referred to as "Dark1", "UV", and "Dark2") to stress-test the photocatalytic film and investigate their stability over a few hours long photocatalytic tests, including dark periods with the inactive photocatalyst immersed in the liquid phase. A constant He flow (10 mL min^{-1}) was bubbled through the liquid phase first under dark conditions to remove dissolved oxygen (until reaching an O_2 background level of 30 ppm in the gas headspace), and then under UV illumination to purge the gaseous products out of the liquid phase to the GC for quantification. The GC was equipped with a Pulsed Discharge Detector (GC-PDD, CompactGC 4.0, Interscience) to measure the concentrations of evolved H_2 (and O_2) with a time resolution of ~ 2 min. Additional details on the experimental setup as well as a sketch of the apparatus can be found in our previous publication. [13] The hydrogen production rate (μmol h^{-1} A_{cat}^{-1}) was calculated according to Eq. 2:

$$Production\ rate = \frac{C_x \bullet j}{V_M \bullet A_{cat}} \quad (2)$$

Where:

- C_x is the concentration of evolved H_2 expressed as part per million (μL L^{-1})
- j is the flow rate of carrier gas (He) expressed in L h^{-1}
- V_m is the molar volume at 298.73 K (24 μL μmol^{-1})
- A_{cat} is the geometric surface area of the photocatalyst layer expressed in cm^{-2}

We calculated the Apparent Quantum Yield according to Eq. 3:

$$AQY(\%) = \frac{2r_{H_2}N_A}{\phi} \times 100 \quad (3)$$

Where:

- r_{H_2} is the hydrogen production rate (mol s^{-1} cm^{-1})
- N_A is the Avogadro number
- ϕ is the photon flux (photons s^{-1} cm^{-2})

2.5. In situ XAS experiments and spectroscopic cell design

In situ XAS fluorescence experiments were performed at the ID26 beamline of the European Synchrotron Radiation Facility (ESRF, Grenoble, France). To study the oxidation state of the Ni, Cu and NiCu co-catalysts under photocatalytic hydrogen evolution conditions we chose the 3d metal K-edges of Cu and Ni, which give direct access to the density of empty 3d states via X-ray Absorption Near Edge Structure (XANES) analysis. The analysis of the pre-edge region of 3d metal K-edges requires high incoming photon flux as well as high energy resolution, making the ERSF ID26 beamline ideal to our objective. Additionally, the use of the 5 analyzing crystal spectrometer installed at ID26 allowed us to acquire spectra for both Ni and Cu K-edges, alternatively, during the same *in situ* experiment. [23] To minimize undesired beam effects, a beam size of 200 μm x 400 μm was used and a scanning pattern was created to acquire each spectrum at a previously unexposed sample location. We used a liquid-phase *in situ* XAS cell similar to the one described in previous work. [13–15] This cell features a thin Mylar front window (01867-AB, SPI, 6 μm), ensuring transparency for both X-rays and UV light. The photocatalyst, fixed on a support, was placed in the cell immersed in either de-ionized water or in a 20 vol% methanol-water mixture. In any case, the liquid phase and the gas headspace in the cell were continuously purged with humidified Ar, hence replicating the experimental conditions outlined above for the photocatalytic reactor, including the UV photon flux and intermittent illumination. A schematic representation and a photograph of the employed cell are reported in Figure S2.

In situ XAS measurements were conducted in fluorescence mode, while reference spectra for Ni (polycrystalline Ni foil and NiO powder pellet) and Cu (polycrystalline Cu foil, and powder pellets of Cu_2O and CuO) were acquired in transmission mode in the −150 eV to + 800 eV range at BM08 beamline of the ESRF. XANES spectra were collected over a photon energy range of −10 to + 80 eV relative to the Ni K-edge (8333 eV) and the Cu K-edge (8978 eV), with a time resolution of ~1 min per spectrum, which enabled us to perform *in situ* time-resolved experiments. To improve the signal-to-noise ratio, groups of 15 and 20 scans of Ni and Cu spectra, respectively, were merged and then fitted using the Athena software. [24] This provides a time resolution of ca. 15 min and 25 min for Ni and Cu spectra, respectively. Some data points in a few experiments had to be discarded (e.g., in Figure S5) due to issues related to an excessively high Ar flow rate, which lead to extremely noisy or distorted spectra. For the study of the spectral peak ratio (details will be introduced in Section 3.2), we averaged 5 spectra to increase the time resolution.

In recent work, [13] we compared the photocatalytic performance of a Ni-STO slurry photocatalyst for water splitting in the photocatalytic reactor and in the *in situ* XAS cell used also in the present work. The comparable photocatalytic performance observed in the two reactors demonstrates that the *in situ* XAS results are relevant to interpret the photocatalytic performance measured with the lab photoreactor.

3. Results and Discussion

3.1. Morphological and crystallographic characterization of materials

The morphology of pristine and co-catalyst coated porous TiO_2 was investigated by SEM. The surface of pristine TiO_2 layers presents pores with average diameter of ~ 80 nm (Fig. 1a), and the cross-section image shows a TiO_2 layer thickness of ~ 8 μm (Fig. 1b). Such thickness was shown in previous work to be optimal for maximized UV light absorption and photocatalytic H_2 production. [16,21]

After the magnetron sputtering deposition, layers of Ni, Cu, and bimetallic NiCu co-catalysts can be observed on top of the porous TiO_2 layers (Fig. 1c-e). No significant difference is observed in the morphology of sputtered thin films of different compositions, and all films (Ni, Cu, and NiCu) appear composed of coalesced nanosized grains.

The phase composition and crystalline features of the annealed photocatalysts were investigated by X-ray Diffraction (XRD). As shown in Fig. 2a, no signal is visible for Ni or Cu phases, and the only visible peaks are attributed to the metallic Ti substrate and TiO_2 layers, the latter present as anatase TiO_2 phase, in line with the annealing conditions (500°C, in air). [1,25] The absence of XRD peaks for the co-catalyst phase can be ascribed to i) the low loading of sputtered co-catalyst [26]

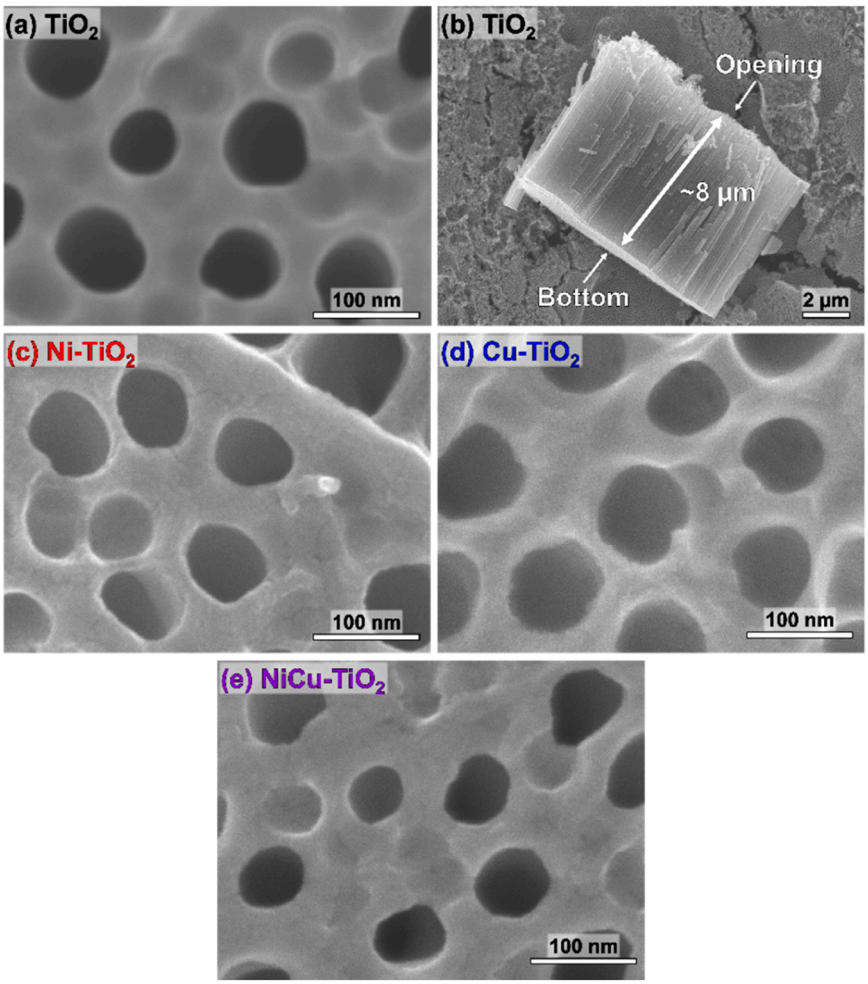

Fig. 1. SEM images of a pristine porous TiO_2 layer: top (a) and cross section (b) views; (c-e) top view SEM images of porous TiO_2 layers coated with Ni, Cu, and NiCu co-catalyst films, respectively.

(in the range of a few 10s µg cm^{-2}) and, possibly, ii) its amorphous or nanocrystalline nature. [16]

To further investigate the co-catalyst films, 100 nm thick Ni and Cu films sputtered onto SiO_2/Si wafers were characterized by grazing angle XRD (Fig. 2b). As shown in Fig. 2b, signals are present at 43.50° for the 111 plane of cubic *Fm*$\bar{3}$*m* Cu and at 44.50° for cubic *Fm*$\bar{3}$*m* Ni, while the peak at 43.95° could be attributed to a NiCu solid solution, as predicted by Vegard's law (Fig. 2c). [2,4,5] The large width of these diffraction peaks indicates the presence of crystalline domains with size of a few nm, in line with what observed in previous reports for room temperature-sputtered Ni and Cu films. [7] The average grain sizes (determined by Scherrer equation) for the 100 nm thick Ni, Cu, and NiCu films are ~ 9 nm, ~ 20 nm, and ~ 11 nm respectively.

3.2. *Photocatalytic activity and in situ XAS experiments*

Fig. 3 compares the photocatalytic activity and the oxide/metal peak ratio of the Ni-, Cu-, and NiCu-TiO_2 photocatalyst films. The oxide/metal peak ratio was obtained from the *in situ* XAS experiments under dark - UV-light illumination (365 nm) - dark conditions, in de-ionized water. [7,41]

The H_2 evolution rate observed for Ni–TiO_2 (Fig. 3a) is nearly double that obtained with Cu–TiO_2 (Fig. 3c). For any photocatalyst, the H_2 production rate begins to increase ~ 2 min after the UV light is switched on, consistent with the estimated delay of 2 min based on the headspace volume of the photocatalytic reactor (CSTR).

No evolved O_2 was detected in any experiment, indicating that the photogenerated holes are consumed in oxidation reactions other than OER - such as water oxidation to hydroxyl radicals [3,6] and/or H_2O_2, [7,27] or co-catalyst oxidation (discussed later). Finally, photogenerated holes might react with defective Ti^{3+} species (typically present in anodic TiO_2) leading to their oxidation to Ti^{4+}, [6] or might oxidize adsorbed carbonaceous species left from the anodization in ethylene glycol. [21,28]

NiCu-TiO_2 outperformed both Ni-TiO_2 and Cu-TiO_2 (Fig. 3e), in line with what reported previously, [16,17,29,30] and with H_2 evolution rates of 0.8, 0.6, and 0.3 µmol h^{-1} cm^{-2}, respectively. For Cu-TiO_2, the H_2 production reached a steady state after approximately 30 min, while for Ni-TiO_2 and NiCu-TiO_2 the H_2 production appeared to slowly increase over time – for Ni-TiO_2, with an increase of ~ 30 nmol h^{-2} cm^{-2}. The obtained hydrogen evolution rates correspond to apparent quantum yields (AQY) of 0.145%, 0.109%, and 0.054%, respectively for NiCu--TiO_2, Ni-TiO_2, and Cu-TiO_2. To identify the active phase of Ni and Cu co-catalysts under reaction conditions and possibly correlate this to the H_2 evolution transients under UV light on/off cycles, we monitored changes in Ni and Cu oxidation state over time by *in situ* XANES.

The co-catalyst films (10 nm thick) were found to cause self-absorption during XAS measurements. This effect, combined with their nanocrystalline nature [7], caused spectral distortions that made the quantification of different Ni and Cu oxidation states unreliable if made by classic approaches, e.g., through Linear Combination Fitting (Figure S3), as used in previous works. [13,14] Various semi-quantitative methods based on spectral features have been

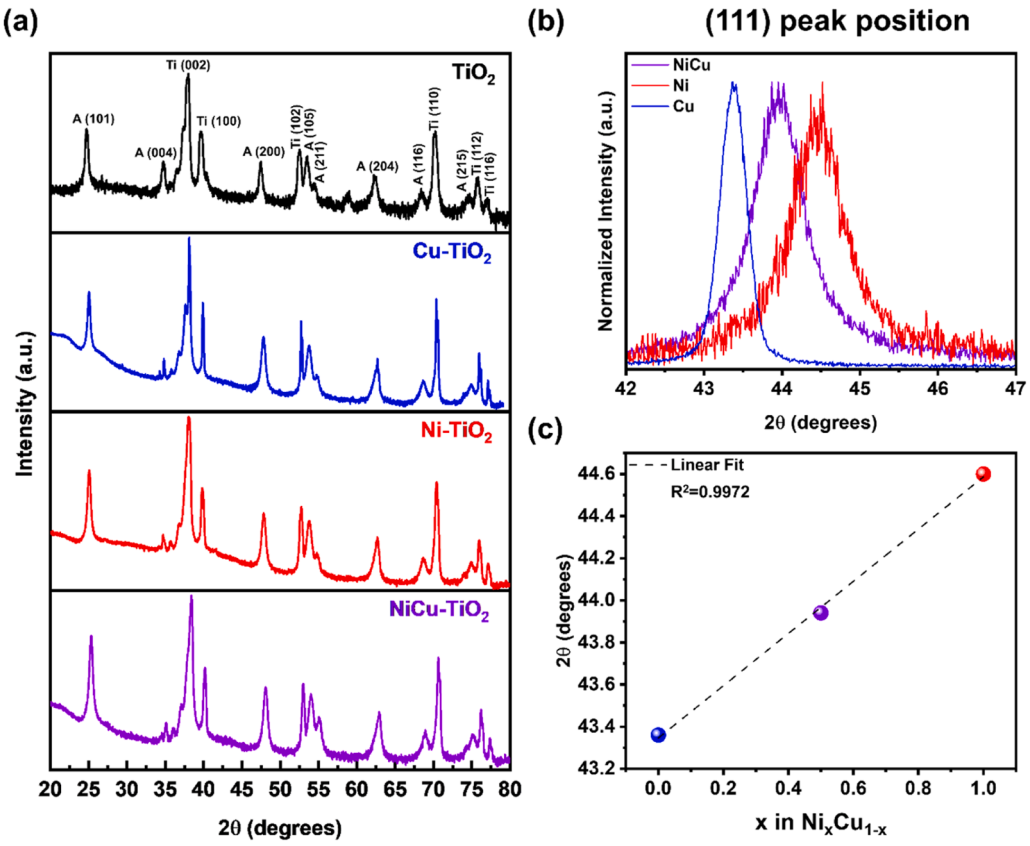

Fig. 2. (a) Diffraction patterns for pristine TiO_2 (black line), Ni-TiO_2 (red line), Cu-TiO_2 (blue line), and NiCu-TiO_2 (purple line); (b) grazing angle diffraction peak (111) for Cu, Ni, and NiCu thin films; (c) position of the 111 peaks for different composition as a function of the Ni content and obtained linear fit (dashed line).

reported in the literature to overcome this issue [31], e.g., calculating the defect density from cell parameters and coordination numbers [32], estimating oxidation state via derivative of μ(E) and subtracting each μ(E) to the absorption spectra of a reference [33], comparing the main peak area and pre-edge shoulder height, analyzing changes in absorption at a specific photon energy (Fixed Energy XAS, FE-XAS) [15], and correlating between signal intensity decrease and material dissolution. [14]

In the present work semi-quantitative analysis of the oxidation states of Ni and Cu, was performed by adopting the following approach: we calculated the intensity ratio between the first and second peaks in each spectra after the absorption edge for both the Ni-K and Cu-K edge spectra, i.e., in an energy region less affected by spectral distortions ascribed to self-absorption or by multiple scattering effects (Figure S4). Metallic Ni and Cu were used as references for the reduced species, while Cu_2O, CuO and NiO served as references for the oxidized species (Cu(I), Cu(II) and Ni(II)).

As an example, we report the analysis for Ni and Cu reference materials in the SI (Figure S4). The absorption values were taken at 8349 eV and 8357 eV for Ni(0), and at 8350 eV and 8365 eV for NiO. For the Cu references, we used 8998 eV and 9007 eV for Cu(0), and 9002 eV and 9020 eV for CuO. As reported in Fig. 3, the peak intensity ratios were close to unity for the metallic foils, while NiO and CuO (+2 oxidation state) showed peak ratios around 2.2, consistent with the characteristic intense white line absorption of oxides. This semi-quantitative approach allowed us to obtain information on the average oxidation state of the co-catalyst films, in terms of relative content of metallic and oxidized phase. A summary of the results is provided in Table S2. All as-prepared photocatalysts present a peak ratio in the 1.4–1.6 range, this indicates that the thin films are composed of a mixture of metal and oxide. This is explained by the oxidation of the outer film layer due to environmental exposure.

To improve data quality while maintaining sufficient time resolution, we averaged 5 spectra to calculate the peak ratio. The calculated peak ratios were then plotted as a function of time and compared to selected Ni and Cu reference materials to determine the oxidation state of the thin films under photocatalytic conditions.

Regarding *in situ* analysis, the thin films exhibited markedly different behaviors, both in the presence and absence of UV illumination. These results suggest different charge transfer dynamics and photocatalytic H_2 evolution mechanisms for the three photocatalyst materials. We plotted the results for the *in situ* spectra as a function of time in Figs. 3b, 3d, and 3 f. While the data trend is consistent for both Ni and Cu throughout the experiment, the noise can be attributed to the scanning mode during the *in situ* XAS experiments. For each scan, a different sample spot is probed, hence each data point reflects minor differences in the local composition and oxidation state of the thin films. Additionally, to provide further insights into the redox dynamics of the Ni and Cu co-catalysts, we examined additional spectral features as detailed in the next sections.

3.2.1. *Detailed spectroscopic analysis of the Ni-TiO_2 photocatalyst*

As shown in Fig. 3b, Ni showed no apparent redox activity upon exposure to plain water in the Dark1. This can be explained by the presence of a "passive" NiO surface phase in the as-prepared sample as discussed above, which may inhibit further oxidation of the buried metallic Ni phase. [34]

Under UV illumination, the Ni co-catalyst film is found to oxidize, reaching a stable peak ratio of ~ 2.1 after approximately 100 min of illumination, indicating that Ni is almost completely oxidized to Ni(II). As shown in Fig. 4a, the metallic features gradually fade off while the white line grows more intense, featuring a spectral shape comparable to that of the NiO reference (Ni(II), see Figure S4b).

Some key spectral differences can be better visualized using derivative spectra. Particularly, a small peak at ~ 8331 eV corresponding to

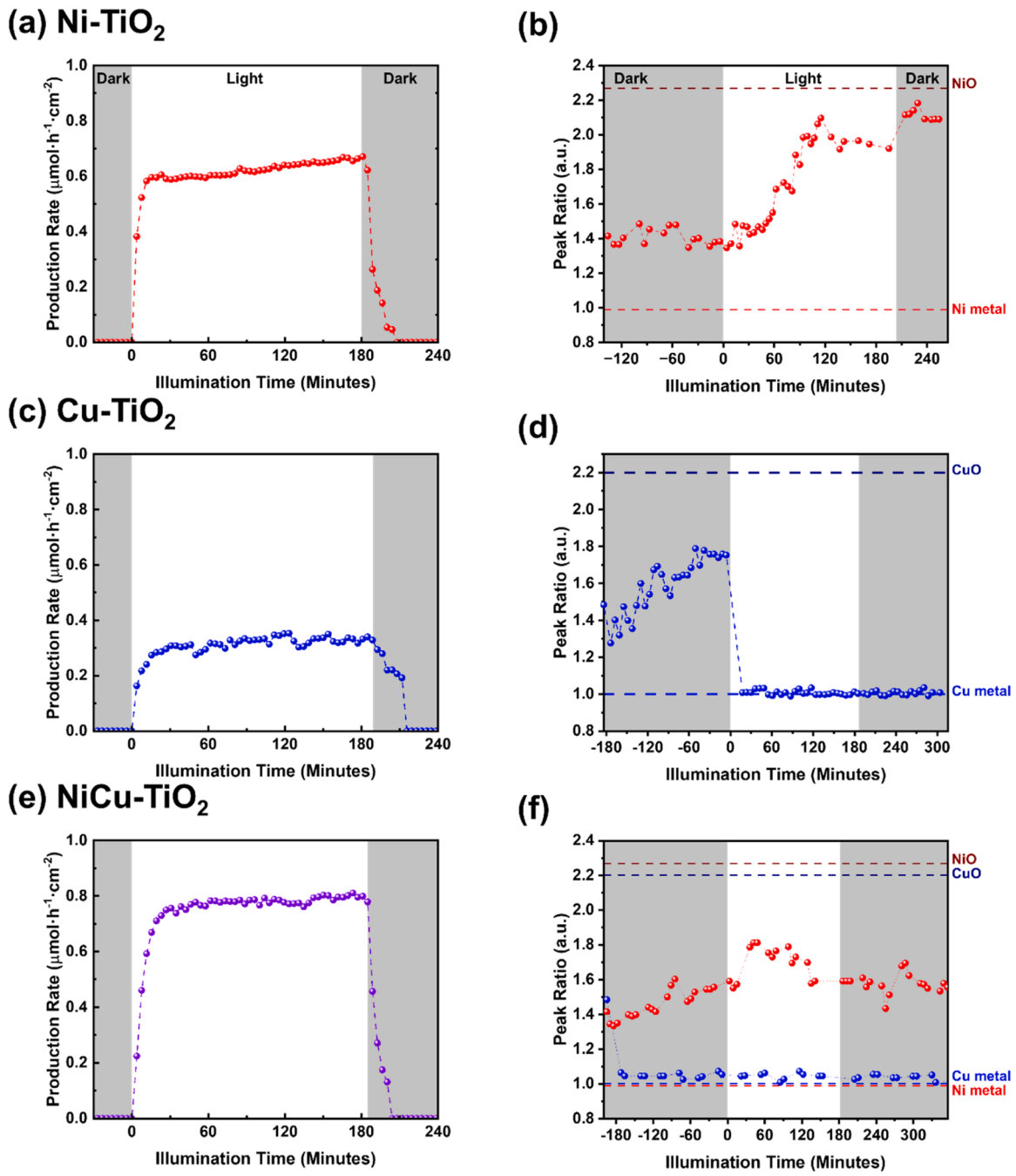

Fig. 3. (a,c,e) Hydrogen evolution rate for (a) Ni-TiO_2, (c) Cu-TiO_2, and (e) NiCu-TiO_2; (b,d,f) Oxide/metal peak ratio for (b) Ni-TiO_2, (d) Cu-TiO_2, and (f) NiCu-TiO_2. Grey areas refer to periods in the dark (absence of UV illumination), while white areas represent UV illumination periods. The dashed horizontal lines represent the calculated ratios for the reference spectra. The selected peaks for ratio analysis were: 8998 eV and 9007 eV for Cu metal, and 9002 eV and 9020 eV for CuO. For Ni metal we employed the 8349 eV and 8357 eV peaks, while for NiO we chose 8350 eV and 8365 eV.

the Ni metal K-edge, and absent in the case of NiO, can be used as an indicator of Ni(0), while the three convoluted peaks between 8335 eV and 8350 eV are representative of Ni(II) (Fig. 4b). By plotting the derivatives of the *in situ* spectra (Fig. 4c-d) we can observe that the peak assigned to the metallic Ni phase reduces in intensity with increasing the UV illumination time, while a broad spectral feature between 8335 eV and 8350 eV gradually appears, confirming a net oxidation of Ni metal to Ni(II). These Ni red-ox dynamics can be visualized also by mapping the intensity of the derivatives spectra over the course of the experiment, as shown in Fig. 4d. Additionally, by integrating the intensity of the peak at ~ 8331 eV (assigned to metallic Ni) over the UV illumination time, one can notice that there are no significant changes in Ni(0) atomic fraction in the absence of UV illumination, whereas this spectral signal shows a clear decay during UV illumination, further confirming the conversion of Ni(0) into an oxidized Ni phase (Ni(II), Fig. 4e).

The behavior of Ni-TiO_2 under UV illumination suggests that holes photogenerated in TiO_2 are, at least partially, transferred to metallic Ni, leading to its oxidation. While this hypothesis aligns well with what has been observed for Ni-NiO core-shell NP-modified $SrTiO_3$, the resulting H_2 evolution transient differs significantly. [13] In the present study, Ni oxidation occurs with no significant impact on the hydrogen evolution rate, which remains steady (or even slightly increases) upon illumination. On the contrary, in the case of Ni-$SrTiO_3$ photocatalysts, co-catalyst oxidation was identified as the primary cause for deactivation.

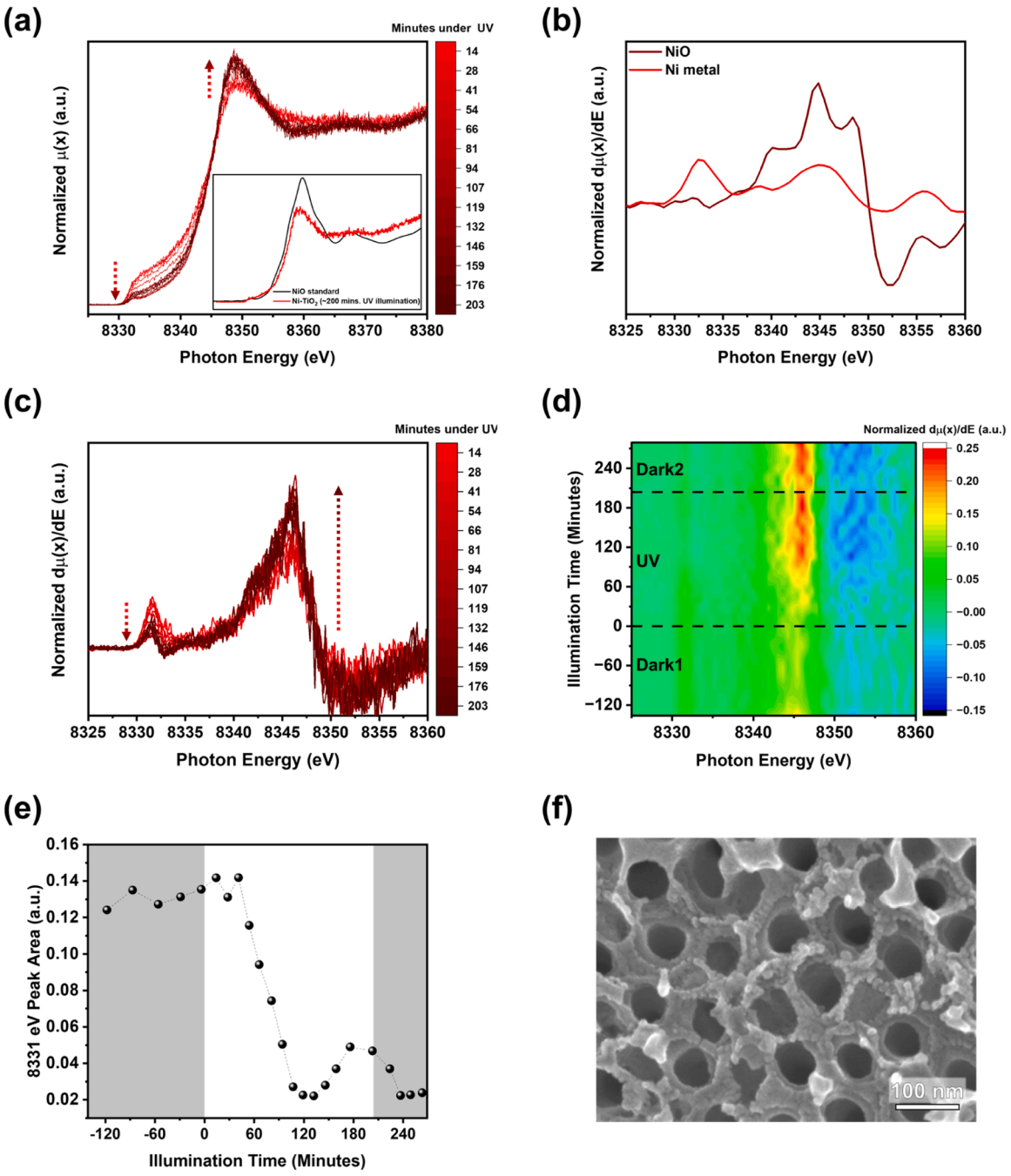

Fig. 4. (a) Time resolved Ni K-edge spectra for Ni-TiO_2 in H_2O under UV illumination; inset: spectrum of Ni(II) standard (black line) compared with the spectra of Ni-TiO_2 after ~200 min of UV illumination to highlight the similarities; (b) derivative spectra for reference phases, i.e., Ni metal and NiO; (c) derivative on the *in situ* spectra; the red dotted arrows are guide to the eye and indicate the spectra evolution over time under illumination; (d) color map of intensity of derivative spectra in (c); (e) integrated area of the peak centered at 8331 eV during photocatalysis; grey areas refer to dark times (Dark1 and Dark2) while white area refer to UV illumination (UV); (f) SEM image of Ni-TiO_2 after photocatalysis (UV illumination in H_2O).

Additionally, changes in Ni oxidation state are accompanied by co-catalyst reconstruction. The SEM image of Ni-TiO_2 after photocatalysis in Fig. 4 f shows that the sputtered Ni film converts into undefined arrangements of nanoparticles – this might take place via a dissolution (Ni→Ni(II)) – redeposition (Ni(II)→Ni) mechanism.

Finally, after switching off the UV light (Dark2), the oxidation state of the Ni co-catalyst does not show further significant changes.

Overall, the spectroscopic analysis shows a net Ni oxidation trend during the first ca. 90 min under UV illumination, while afterwards the Ni oxidation state remains relatively constant – see data in Figs. 3b and 4e.

The photocatalytic results in Fig. 3a show an almost steady photocatalytic activity for Ni-TiO_2, with only a slight increase of the H_2 evolution rate over UV time of ~ 0.6 μmol h^{-2} cm^{-2}. To produce H_2, the photocatalyst needs i) either metallic Ni species to transfer CB electrons from TiO_2 to reduce water (Eq. 4), or ii) metallic Ni species to react with water forming oxidized Ni(II) species and H_2 (Eq. 5). At the same time, unselective charge extraction might cause Ni oxidation via VB holes (Eq. 6). Oxidized Ni species (Ni(II)) formed via Eqn 6 can reduce back to metallic Ni via CB electrons (Eq. 7).

$$2H_2O_{(l)} + 2e^-_{CB} \xrightarrow{Ni^0} H_{2(g)} + 2OH^-_{(aq)} \quad (4)$$

$$Ni_{(s)} + H_2O_{(l)} \rightarrow NiO_{(s)} + H_{2(g)} \quad (5)$$

$$Ni_{(s)} + 2h^+_{VB} \rightarrow Ni(II)_{(s)} \quad (6)$$

$$NiO_{(s)} \left[or\ Ni(II)_{(s)} \right] + 2e^-_{CB} \rightarrow \quad Ni_{(s)} \quad (7)$$

Based on the almost steady H_2 evolution rate, we propose a dynamic Ni oxidation – Ni(II) reduction equilibrium in the co-catalyst phase. Ni oxidation to Ni(II) might dominate over the reverse process (Ni(II) reduction) at the beginning of UV illumination, in line with the increasing peak ratio as derived from the *in situ* XAS spectra. Subsequently, Ni oxidation and Ni(II) reduction might proceed at comparable rates (dynamic equilibrium), and the average Ni oxidation state does not show significant net changes, resulting in a stable peak ratio. The dynamic equilibrium is accompanied by co-catalyst reconstruction, from a thin film morphology into nanoparticles. This reconstruction is likely due to Ni-to-Ni(II) oxidation and dissolution (Eqs. 5 and 6) followed by Ni(II)-to-Ni photo-deposition via TiO_2 CB electrons (Eq. 7).

3.2.2. Detailed spectroscopic analysis of the Cu-TiO_2 photocatalyst

For Cu-TiO_2, we observe that during Dark1 (~ 2.5 h), Cu undergoes slight oxidation, as shown by the increase in CuO/Cu peak ratio from ~ 1.4 to ~ 1.8 (Fig. 3d) as well as from the shape of the *in situ* spectra (Fig. 5a). By analyzing the pre-edge features, we observe that the peak centered at ~8989 eV, characteristic of Cu (II), increases gradually over time (Fig. 5b-c). By examining the derivative of the Cu, Cu_2O and CuO reference spectra (Fig. 5d), we can identify key markers distinguishing different Cu species. The strongest peak, corresponding to the absorption edge, shifts to higher photon energy when the oxidation state increases, specifically from ~8980 eV for metallic Cu to ~8988 eV for CuO. Additionally, the CuO derivative spectrum exhibits another intense peak at 8995 eV, which is stronger than in metallic Cu and Cu_2O.

The derivative spectra of the as-prepared photocatalyst (Fig. 5e) display features that are characteristic of all three reference spectra, likely due to partial oxidation of the sputtered metallic Cu upon air exposure. A small peak at 8978 eV suggests the presence of CuO, while two overlapping peaks between 8980 eV and 8985 eV indicate contributions from metallic Cu and Cu_2O. Additionally, a peak at 8988 eV, associated with CuO, overlaps with the characteristic double peak feature of Cu_2O observed between 8987 eV and 9000 eV.

During the first 30 min in water without UV illumination (Dark1), the spectral features of the Cu-based co-catalyst resemble a combination of Cu and Cu_2O, consistent with a low intensity of the pre-edge peak at 8979 eV (Fig. 5b-c). However, as immersion time increases, the derivative spectra exhibit more pronounced CuO features. Specifically, the peaks at 8979 eV and 8987 eV intensify, while the convoluted peaks at 8980 eV and 8985 eV become smaller (Fig. 5e-f).

These results suggest that, in contact with water (Dark 1), the copper co-catalyst phase oxidizes due to the oxidation of surface exposed metallic Cu in water in the presence of dissolved oxygen. The latter might be present at the beginning of Dark1 – while inert gas purging throughout Dark1 ensures that oxygen is not present in the liquid phase when UV illumination is started (UV). This behavior is reversed under UV illumination. Cu is reduced, reaching a peak ratio of 1 (i.e., 100% metallic Cu phase) within 15 min after starting the UV illumination (Fig. 3d). In fact, once UV is turned on, the intensity of the metallic Cu feature (~ 8978 eV) suddenly rises, while that of CuO decreases.

To summarize, the *in situ* XAS results for Cu-TiO_2 under UV illumination suggest the transfer of CB electrons from TiO_2 to the Cu-based co-catalyst, causing its complete reduction to a Cu metallic phase, in line with previous literature. [23,35,36] A metal-semiconductor (Schottky) junction forms, enabling electron transfer to the metallic Cu co-catalyst, which functions as active site for the hydrogen evolution reaction (HER). [14]

As discussed for Ni-TiO_2, also for Cu-TiO_2 no evolved O_2 gas could be detected. This suggests that holes might [37] react with water forming undetected products (e.g., OH* radicals or H_2O_2) [7,27] or oxidize carbonaceous species adsorbed on TiO_2 due to anodization in ethylene glycol. [21,28]

Interestingly, the morphology of the co-catalyst layer does not show significant changes over the course of the reaction (Fig. 5 h), possibly because red-ox processes might only involve the surface of the co-catalyst film, and Cu oxide does not dissolve in water.

3.2.3. Detailed spectroscopic analysis of the NiCu-TiO_2 photocatalyst

The beamline ID26 at ESRF makes it possible to monitor both the Ni and Cu K-edges in an alternating fashion during a single *in situ* experiment (Fig. 3 f). The results overall indicate that the Ni phase behaves differently in NiCu-TiO_2 compared to Ni-TiO_2 (Fig. 3b) while *in situ* Cu spectra do not show significant differences when comparing NiCu-TiO_2 with Cu-TiO_2 (Fig. 3d).

The Ni phase in the bimetallic co-catalyst appears to gradually oxidize during the ~ 3 h-long dark period in water. The peak ratio increases from ~ 1.3 to ~ 1.6. Under UV illumination, the peak ratio varies over time reaching values as high as ~ 1.8, suggesting further oxidation of the Ni phase under UV illumination. Data scattering might be ascribed to the scanning pattern, i.e., each scan probes a different sample spot, hence data may reflect differences in the local composition and oxidation state of the co-catalyst films. It is however evident that the Ni phase in the bimetallic co-catalyst does not oxidize as much as in Ni-TiO_2 (max peak ratio of ~ 1.8 for Ni-TiO_2 vs. ~ 2.1 for NiCu-TiO_2 after 180 min-long UV irradiation).

This lower average oxidation state of the Ni phase in NiCu-TiO_2 compared to Ni-TiO_2 suggests that holes photogenerated in TiO_2 are more efficiently transferred to the liquid phase (e.g., forming OH* radicals or H_2O_2) and contribute less to co-catalyst oxidation. [14,16,26,38] Additionally, the work function and Fermi level of bimetallic co-catalysts varies with their composition, and the presence of Cu makes the co-catalyst phase less prone to oxidation compared to monometallic Ni co-catalysts. [39] The average oxidation state of the Ni phase in the subsequent period in the dark (Dark2) remains stable at ~ 1.6, with no consistent trend. Also in this case, data scattering can be ascribed to the scanning pattern.

On the contrary, the average oxidation state for the Cu phase decreases from ~ 1.5 to ~ 1.0 within ~ 30 min upon immersion in water in the dark. This suggests the dissolution of surface Cu oxides along with diffusion of solvated Cu ions away from the probing beam. This is the reason behind the decrease in the overall peak ratio, which should not be considered as a cathodic process, but a net decrease in the concentration of oxidized Cu species in the probed photocatalyst spot. In addition, we should consider the co-existence of both Ni and Cu phases in the co-catalyst. Ni is "less noble", i.e., more easily oxidized in water than Cu ($E^0_{Ni^{2+}/Ni} = -0.23V\ vs.\ E^0_{Cu^{2+}/Cu} = +0.34V vs.\ SHE$). The galvanic coupling may also explain the reduction of Cu and simultaneous oxidation of Ni.

To further analyze the *in situ* Ni spectra, we mapped changes in the derivative of the absorption coefficient over illumination time (Fig. 6a-b). We observe an initial increase in the wide peak at ~ 8350 eV during Dark1, indicating gradual oxidation. Under UV illumination, oxidation is more significant as shown by both the color map (Fig. 6b) and the peak integration at 8331 eV (Fig. 6c). As observed for Ni-TiO_2 (Fig. 4 f), light-induced oxidation of Ni causes significant co-catalyst reconstruction also for NiCu-TiO_2 (Fig. 6d). By comparing the morphology of NiCu-TiO_2 after photocatalysis with the monometallic systems, it is reasonable to assume that the major cause for reconstruction is Ni oxidation (while Cu-TiO_2 does not undergo significant changes – Fig. 5 f).

Based on these results and by comparison with the behavior of monometallic systems, we propose that the photocatalytic mechanism suggested for Ni-TiO_2 applies also for NiCu-TiO_2, except that the bimetallic co-catalyst enables improved charge transfer and faster H_2

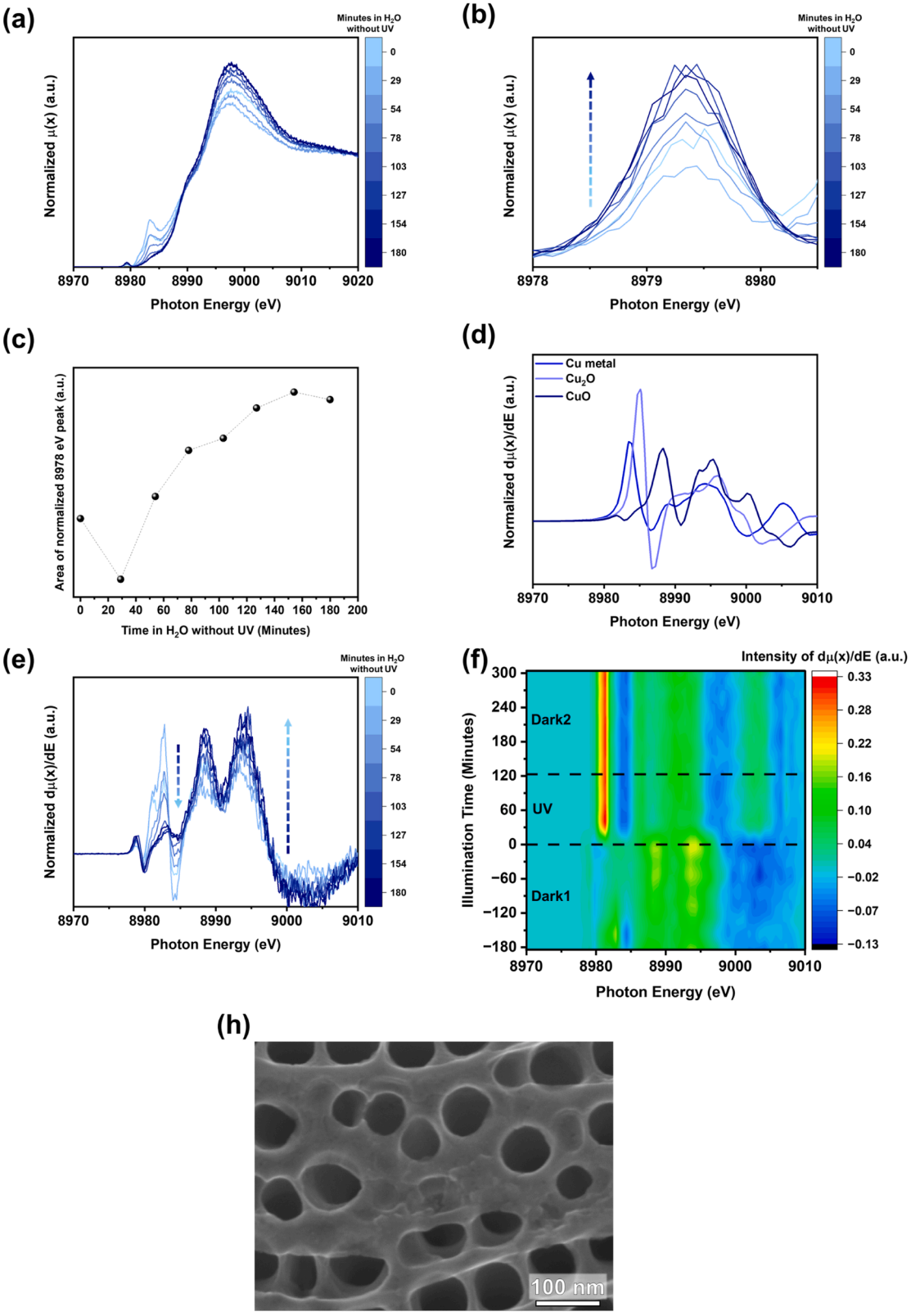

Fig. 5. (a) Time resolved Cu K-edge spectra of Cu-TiO_2 during Dark1 period; (b) inset highlighting the intensity of the pre-edge peak at ~8979 eV; (c) integrated intensity of the peak in (b); (d) derivatives spectra of the reference; (e) *in situ* derivative spectra during Dark1; (f) color map of intensity of derivative over the course of the reaction; (h) SEM image of Cu-TiO_2 after photocatalysis (UV illumination in H_2O).

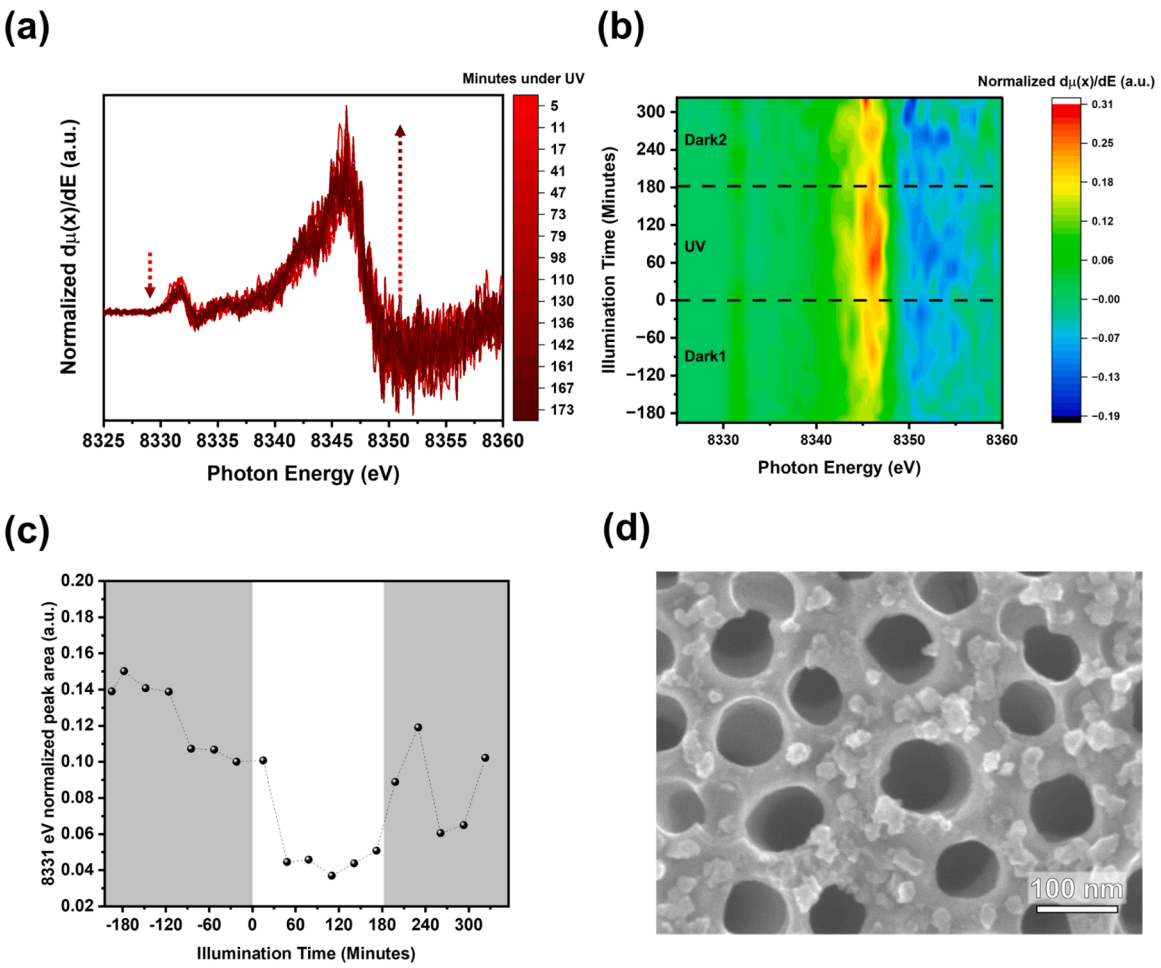

Fig. 6. (a) Time resolved spectra at the Ni K-edge for NiCu-TiO2 in H2O during UV illumination; (b) integrated area of the derivative peak at ~8331 eV during the reaction; (b) color map of intensity of derivative spectra at the Ni-K edge during the reaction (d) SEM micrography of NiCu-TiO_2 after photocatalysis (UV illumination in H_2O).

evolution kinetics. regarding the role of Cu in the photocatalytic process, we cannot exclude that, as in the case of Cu-TiO_2, photogenerated electrons contribute to H_2 evolution also through electron transfer via the metallic Cu phase.

3.2.4. *Photocatalysis in MeOH-H_2O*

After assessing mono- and bimetallic co-catalysts in plain water, we further investigated the most active photocatalyst, namely NiCu-TiO_2, in a 20% MeOH-H_2O mixture. Under alcohol reforming conditions, MeOH acts as a hole scavenger, leading to higher H_2 evolution rates. We aimed to investigate how the reaction medium, i.e., plain water vs. methanolic solution, affects the oxidation of the co-catalyst, under UV light on/off cycles.

The H_2 evolution transient is shown in Fig. 7a, along with the *in situ* XAS results in Fig. 7b (Ni and Cu peak ratio over reaction time).

A slow decrease in the Ni peak ratio from ~ 1.4 to ~ 1.2 is observed during the dark period in MeOH-H_2O. Most importantly, and differently from what is observed in plain water, the Ni phase does not undergo oxidation under UV illumination. Instead, it appears that the content of metallic Ni phase in the co-catalyst slightly increases during photocatalysis. This is visible from the spectral features of the derivatives' spectra in Fig. 7c,d. After turning on the UV light, the peak at 8331 eV, typical of metallic Ni, increases in intensity (Fig. 7c), and its integrated area increases (Fig. 7d). After turning off UV, no significant change in the spectral features can be observed. Similarly, the Cu phase in the co-catalyst reaches a peak ratio of ~ 1.0 within 30 min after immersion in MeOH-H_2O in the dark. Afterwards, the average oxidation state of the Cu phase remains unchanged both under UV illumination and during the subsequent dark period (Fig. 7b). For both Ni and Cu phases, the net decrease in oxidation state can be attributed to the dissolution of surface oxides upon immersion in MeOH-H_2O – dissolution and diffusion of ions away from the probed area leads to the decrease of the peak ratio.

The results overall suggest an effective scavenging of photo-holes by MeOH, which prevents co-catalyst oxidation. Effective scavenging of photo-holes is indirectly confirmed by a ca. 50 times higher H_2 evolution rate compared to what measured for the same photocatalyst in plain water (~ 40 vs. ~ 0.8 μmol h^{-1} cm^{-2}). As control experiments, we performed *in situ* XAS analysis in the same experimental conditions for Ni-TiO_2 and Cu-TiO_2 (Figure S5). Similar trends in peak ratios are observed for monometallic systems, indicating that Ni and Cu monometallic co-catalysts on TiO_2 behave comparably to a bimetallic NiCu system. Furthermore, this suggests that galvanic coupling has minor effects on redox dynamics of bimetallic NiCu co-catalysts under photoreforming conditions, i.e., in the presence of a hole scavenger.

4. Conclusions

We used *in situ* XAS to investigate the oxidation state of monometallic Ni and Cu, and bimetallic NiCu phases as TiO_2 co-catalysts for photocatalytic H_2 evolution from plain water and water-methanol solutions. The results of photocatalytic H_2 evolution experiments confirmed the co-catalyst activity trend known from previous studies, i.e., NiCu-TiO_2

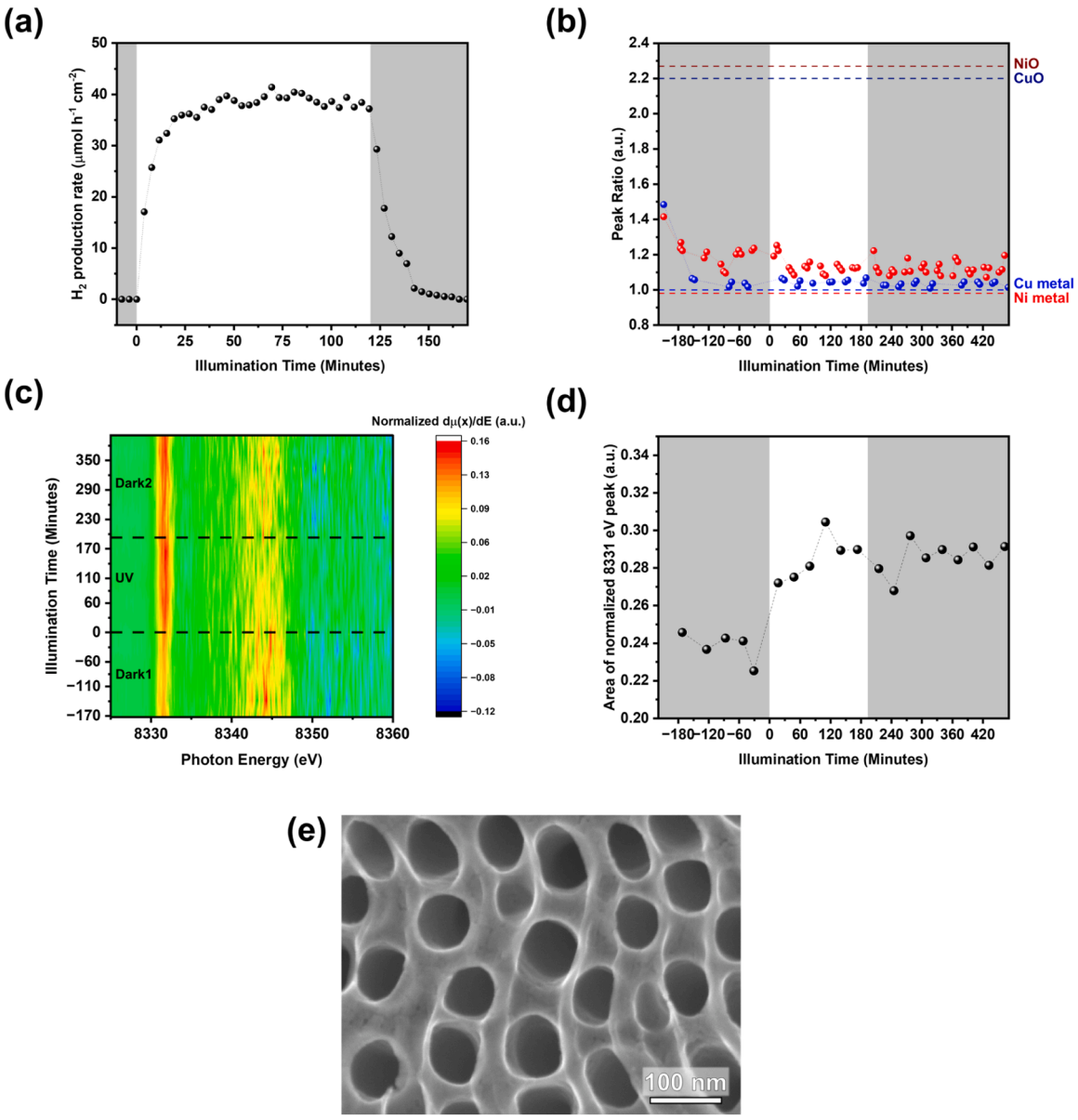

Fig. 7. (a) HER production rate for NiCu-TiO_2; (b) peak ratio for Ni (red) and Cu (blue) over the course of the photocatalytic process; (c) intensity of the derivatives' spectra of Ni over the course of the reaction; (d) integrated area of the derivative 8331 eV peak; (e) SEM image of NiCu-TiO_2 after photocatalysis (UV illumination in a 20% MeOH-H_2O mixture).

> Ni-TiO_2 > Cu-TiO_2. To address spectral distortions due to co-catalyst self-absorption effects and their nanocrystalline nature, we used a semi-quantitative method based on spectra peaks' ratio. This enabled us to monitor changes in Ni and Cu oxidation state over time and, more importantly, to identify the active phase of Ni and Cu co-catalysts under reaction conditions. We analyzed the time-resolved XAS spectra in relation to H_2 evolution transients upon UV light off/on/off cycles and changes in co-catalyst morphology. Combining these complementary experimental methodologies, we formulated a hypothesis on charge carrier dynamics, catalyst surface reconstruction and nature of active sites for Ni-, Cu-, and NiCu-TiO_2 photocatalysts.

Overall, the results highlight the complex and dynamic behavior of Ni and Cu co-catalysts under photocatalytic H_2 evolution conditions. In addition to dark processes (e.g., co-catalyst dissolution) and redox dynamics induced by photo-generated charge carriers (co-catalyst oxidation vs. reduction), galvanic coupling in bimetallic co-catalyst and the presence of a hole-scavenger are found to substantially affect the co-catalysts' oxidation state and their changes under intermittent illumination.

As in photocatalytic systems the sites for anodic and cathodic reactions can coexist within nm-scale distances, the oxidation state of the co-catalyst can be affected by both hole and electron transfers – particularly when the co-catalyst is unselectively deposited on both electron- and hole-transfer sites of the photocatalyst. Therefore, redox dynamics of Ni and Cu co-catalysts are yet to be fully understood. The present work, however, underpins the importance of method development in the field of *in situ* (X-ray) spectroscopy, and lays a further step towards unveiling photocatalytic mechanism and the active phase of co-catalysts "at work". As developed in the present study, the *in situ* XAS method proposed does not yet allow to correlate intermediate peak ratio values (*i.e.*, between the minima (pure metallic phase) and the maxima (pure oxidic phase)) to the exact phase composition. It is however foreseen that full quantitative analysis can be achieved by analyzing reference samples with known metallic and oxidic phase composition, which can be used to derive a calibration over the entire range of peak ratio values, from the minimum (100% metallic phase) to the maximum

(100% oxidic phase).

CRediT authorship contribution statement

Marco Pinna: Writing – review & editing, Writing – original draft, Visualization, Validation, Methodology, Investigation, Formal analysis, Data curation, Conceptualization. **MemetTursun Abudukade:** Writing – review & editing, Writing – original draft, Visualization, Validation, Methodology, Investigation, Formal analysis, Data curation, Conceptualization. **Viktoriia A. Saveleva:** Writing – review & editing, Methodology, Investigation, Conceptualization. **Davide Spanu:** Writing – review & editing. **Xiufang He:** Investigation. **Sandro Recchia:** Writing – review & editing, Resources. **Alessandro Minguzzi:** Writing – review & editing, Resources.**Guido Mul:** Writing – review & editing, Resources. **Paolo Ghigna:** Writing – review & editing, Validation, Supervision, Methodology, Formal analysis, Data curation, Conceptualization. **Marco Altomare:** Writing – review & editing, Writing – original draft, Visualization, Validation, Supervision, Resources, Project administration, Methodology, Investigation, Funding acquisition, Formal analysis, Data curation, Conceptualization.

Declaration of Competing Interest

The authors declare the following financial interests/personal relationships which may be considered as potential competing interests: Marco Altomare reports equipment was provided by European Synchrotron Radiation Facility (ESRF). Marco Altomare reports financial support was provided by German Research Foundation (Deutsche Forschungsgemeinschaft DFG). Marco Altomare reports financial support was provided by Dutch Research Council (Nederlandse Organisatie voor Wetenschappelijk Onderzoek NWO). Alessandro Minguzzi reports financial support was provided by Piano di Sostegno alla Ricerca 2025 (Linea 2 A). If there are other authors, they declare that they have no known competing financial interests or personal relationships that could have appeared to influence the work reported in this paper.

Acknowledgements

We acknowledge the European Synchrotron Radiation Facility (ESRF) for provision of synchrotron radiation facilities under proposal ID CH−6517 and on beamline ID26. M.T.A. and M.A. acknowledge financial support from the German Research Foundation (Deutsche Forschungsgemeinschaft DFG, project no. DFG-grant AL 2479/1–1) and the Dutch Research Council (Nederlandse Organisatie voor Wetenschappelijk Onderzoek NWO, project no. ECCM.TT.ECCM.005). We thank the Membrane Science and Technology (MST), Inorganic Materials Science (IMS), and XUV Optics groups of the University of Twente for access to SEM, XRR, and grazing-angle XRD. A.M. is grateful to Piano di Sostegno alla Ricerca 2025 (Linea 2 A) – Università degli Studi di Milano.

Appendix A. Supporting information

Supplementary data associated with this article can be found in the online version at doi:10.1016/j.apcata.2026.121065.

Data availability

Data will be made available on request.

References

[1] S.P. Albu, H. Tsuchiya, S. Fujimoto, P. Schmuki, TiO 2 Nanotubes – Annealing Effects on Detailed Morphology and Structure, Eur. J. Inorg. Chem. 2010 (2010) 4351–4356.
[2] L. Vegard, Die Konstitution der Mischkristalle und die Raumfüllung der Atome, Z. F. üR. Phys. 5 (1921) 17–26.
[3] L. Zhang, Q. Liu, T. Aoki, P.A. Crozier, Structural Evolution during Photocorrosion of Ni/NiO Core/Shell Cocatalyst on TiO 2, J. Phys. Chem. C. 119 (2015) 7207–7214.
[4] L. De Rogatis, T. Montini, B. Lorenzut, P. Fornasiero, NixCuy/Al2O3 based catalysts for hydrogen production, Energy Environ. Sci. (2008), https://doi.org/10.1039/b805426f.
[5] Z. Lin, J. Li, L. Li, L. Yu, W. Li, G. Yang, Manipulating the hydrogen evolution pathway on composition-tunable CuNi nanoalloys, J. Mater. Chem. A Mater. 5 (2017) 773–781.
[6] E. Wierzbicka, E. Szaniawska-Białas, T. Schultz, A.O. Basilio, D. Siemiaszko, K. Ray, N. Koch, N. Pinna, M. Polański, Long-Term Stability of Light-Induced Ti3+ Defects in TiO2 Nanotubes for Amplified Photoelectrochemical Water Splitting, ChemSusChem 17 (2024) e202301614.
[7] V.M. Daskalaki, P. Panagiotopoulou, D.I. Kondarides, Production of peroxide species in Pt/TiO2 suspensions under conditions of photocatalytic water splitting and glycerol photoreforming, Chem. Eng. J. 170 (2011) 433–439.
[8] K. Wenderich, M. Altomare, Sustainable Nanomaterials for Energy Applications, 71, IOP Publishing, 2023, pp. 6-1–6-6.
[9] K. Domen, A. Kudo, T. Onishi, Mechanism of photocatalytic decomposition of water into H2 and O2 over NiO□SrTiO3, J. Catal. 102 (1986) 92–98.
[10] T.K. Townsend, N.D. Browning, F.E. Osterloh, Overall photocatalytic water splitting with NiOx–SrTiO3 – a revised mechanism, Energy Environ. Sci. 5 (2012) 9543.
[11] K. Domen, A. Kudo, T. Onishi, N. Kosugi, H. Kuroda, Photocatalytic decomposition of water into H2 and O2 over NiO-SrTiO3 powder. 1. Structure of the catalyst, J. Phys. Chem. 90 (1986) 292–295.
[12] M.J. Muñoz-Batista, D. Motta Meira, G. Colón, A. Kubacka, M. Fernández-García, "Phase-Contact Engineering in Mono- and Bimetallic Cu-Ni Co-catalysts for Hydrogen Photocatalytic, Mater. " Angew. Chem. Int. Ed. 57 (2018) 1199–1203.
[13] M.T. Abudukade, M. Pinna, D. Spanu, G. De Amicis, A. Minguzzi, A. Vertova, S. Recchia, P. Ghigna, G. Mul, M. Altomare, Situ X-ray Absorption Spectroscopy Study of the Deactivation Mechanism of a Ni-SrTiO3 Photocatalyst Slurry Active in Water Splitting, J. Phys. Chem. C. (2024), https://doi.org/10.1021/acs.jpcc.4c04688.
[14] D. Spanu, A. Minguzzi, S. Recchia, F. Shahvardanfard, O. Tomanec, R. Zboril, P. Schmuki, P. Ghigna, M. Altomare, An Operando X-ray Absorption Spectroscopy Study of a NiCu−TiO 2 Photocatalyst for H 2 Evolution, ACS Catal. 10 (2020) 8293–8302.
[15] M. Altomare, S. Qin, V.A. Saveleva, Z. Badura, O. Tomanec, A. Mazare, G. Zoppellaro, A. Vertova, A. Taglietti, A. Minguzzi, P. Ghigna, P. Schmuki, Metastable Ni(I)-TiO 2− x Photocatalysts: Self-Amplifying H 2 Evolution from Plain Water without Noble Metal Co-Catalyst and Sacrificial Agent, J. Am. Chem. Soc. 145 (2023) 26122–26132.
[16] M. Pinna, A.W.W. Wei, D. Spanu, J. Will, T. Yokosawa, E. Spiecker, S. Recchia, P. Schmuki, M. Altomare, Amorphous NiCu Thin Films Sputtered on TiO2 Nanotube Arrays: A Noble-Metal Free Photocatalyst for Hydrogen Evolution, ChemCatChem 14 (2022), https://doi.org/10.1002/cctc.202201052.
[17] D. Spanu, S. Recchia, S. Mohajernia, O. Tomanec, Š. Kment, R. Zboril, P. Schmuki, M. Altomare, Templated dewetting-alloying of NiCu Bilayers on TiO2 nanotubes enables efficient noble-metal-free photocatalytic H2 evolution, ACS Catal. 8 (2018) 5298–5305.
[18] M. Altomare, K. Lee, M.S. Killian, E. Selli, P. Schmuki, Ta-Doped TiO 2 Nanotubes for Enhanced Solar-Light Photoelectrochemical Water Splitting, Chem. A Eur. J. 19 (2013) 5841–5844.
[19] O. Zakir, A. Ait-Karra, R. Idouhli, M. Khadiri, B. Dikici, A. Aityoub, A. Abouelfida, A. Outzourhit, A review on TiO2 nanotubes: synthesis strategies, modifications, and applications, J. Solid. State Electrochem. 27 (2023) 2289–2307.
[20] P. Roy, S. Berger, P. Schmuki, 2011, DOI: 10.1002/anie.201001374.
[21] G. Cha, P. Schmuki, M. Altomare, Free-Standing Membranes to Study the Optical Properties of Anodic TiO2 Nanotube Layers, Chem. Asian J. 11 (2016) 789–797.
[22] J. Zhang, S. Yan, S. Zhao, Q. Xu, C. Li, Photocatalytic activity for H2 evolution of TiO2 with tuned surface crystalline phase, Appl. Surf. Sci. 280 (2013) 304–311.
[23] B. Xin, P. Wang, D. Ding, J. Liu, Z. Ren, H. Fu, Effect of surface species on Cu-TiO 2 photocatalytic activity, Appl. Surf. Sci. 254 (2008) 2569–2574.
[24] B. Ravel, M. Newville, J. Synchrotron Radiat. (2005) 537–541.
[25] M. Altomare, M. Pozzi, M. Allieta, L.G. Bettini, E. Selli, H2 and O2 photocatalytic production on TiO2 nanotube arrays: Effect of the anodization time on structural features and photoactivity, Appl. Catal. B (2013) 81–88. *136–137*.
[26] J. Sinfelt, J. Carter, D. Yates, Catalytic hydrogenolysis and dehydrogenation over copper-nickel alloys, J. Catal. 24 (1972) 283–296.
[27] L. Wang, S. Cao, K. Guo, Z. Wu, Z. Ma, L. Piao, Simultaneous hydrogen and peroxide production by photocatalytic water splitting, Chin. J. Catal. 40 (2019) 470–475.
[28] M.Z. Ge, C.Y. Cao, J.Y. Huang, S.H. Li, S.N. Zhang, S. Deng, Q.S. Li, K.Q. Zhang, Y. K. Lai, Synthesis, modification, and photo/photoelectrocatalytic degradation applications of TiO2 nanotube arrays: A review, Nanotechnol. Rev. 5 (2016) 75–112.
[29] I. Majeed, M.A. Nadeem, E. Hussain, G.I.N. Waterhouse, A. Badshah, A. Iqbal, M. A. Nadeem, H. Idriss, On the Synergism between Cu and Ni for Photocatalytic Hydrogen Production and their Potential as Substitutes of Noble Metals, ChemCatChem 8 (2016) 3146–3155.
[30] K. Divyarani, S. Sreenivasa, V.S. Anusuaya devi, M.S. Raghu, T.M.C. Rao, F. Alharethy, B.-H. Jeon, P. Martis, S. Kumar, L. Parashuram, An efficient novel NiCu@INA/rGO MOF hollow microsphere Z-scheme heterojunction catalyst for the photocatalytic degradation of tetracycline and simultaneous degradation of

cationic and anionic Dyes" *Colloids Surf*, A Physicochem. Eng. Asp. 703 (2024) 135415.
[31] Á. Muñoz-Noval, K. Fukami, A. Koyama, T. Kuruma, S. Hayakawa, "In situ semi-quantitative analysis of zinc dissolution within nanoporous silicon by X-ray absorption fine-structure spectroscopy employing an X-ray compatible cell", J. Synchrotron Radiat. 26 (2019) 119–123.
[32] J. Ren, H. Chi, L. Tan, Y.K. Peng, G. Li, M. Meng-Jung Li, Y. Zhao, X. Duan, 2023, Royal Society of Chemistry preprint, DOI: 10.1039/d2ta09033c.
[33] M. Coduri, P. Masala, L. Del Bianco, F. Spizzo, D. Ceresoli, C. Castellano, S. Cappelli, C. Oliva, S. Checchia, M. Allieta, D.V. Szabo, S. Schlabach, M. Hagelstein, C. Ferrero, M. Scavini, Local structure and magnetism of Fe2O3 maghemite nanocrystals: The role of crystal dimension, Nanomaterials 10 (2020), https://doi.org/10.3390/nano10050867.
[34] L.-F. Huang, M.J. Hutchison, R.J. Santucci, J.R. Scully, J.M. Rondinelli, Improved Electrochemical Phase Diagrams from Theory and Experiment: The Ni–Water System and Its Complex Compounds, J. Phys. Chem. C. 121 (2017) 9782–9789.
[35] M. González-Tejero, J.G. Villachica-Llamosas, A. Ruiz-Aguirre, G. Colón, "High-Performance Photocatalytic H2 Production Using a Binary Cu/TiO2/SrTiO3 Heterojunction", ACS Appl. Energy Mater. 6 (2023) 4007–4015.
[36] M. Janczarek, E. Kowalska, 2017, MDPI preprint, DOI: 10.3390/catal7110317.
[37] M.A. Mannaa, K.F. Qasim, F.T. Alshorifi, S.M. El-Bahy, R.S. Salama, Role of NiO Nanoparticles in Enhancing Structure Properties of TiO2and Its Applications in Photodegradation and Hydrogen Evolution, ACS Omega 6 (2021) 30386–30400.
[38] D.A. Cadenhead, N.J. Wagner, Low-temperature hydrogen adsorption on copper-nickel alloys, J. Phys. Chem. 72 (1968) 2775–2781.
[39] R. Ishii, K. Matsumura, A. Sakai, T. Sakata, Work function of binary alloys, Appl. Surf. Sci. 169 (170) (2001) 658–661.